Droplet Splashing on an Inclined Surface

Jiguang Hao,[1,*] Jie Lu,[1] Liaonan Lee,[1] Zhihu Wu,[1] Gengkai Hu,[1] and J. M. Floryan[2]
[1]*School of Aerospace Engineering, Beijing Institute of Technology, Beijing 100081, China*
[2]*Department of Mechanical and Materials Engineering, The University of Western Ontario, London, Ontario N6A 5B9, Canada*

(Received 24 October 2018; revised manuscript received 19 December 2018; published 5 February 2019)

Oblique droplet impacts onto a smooth surface at various inclination angles and at different ambient gas pressures were investigated using high-speed photography. It was found that the droplet splash can be entirely suppressed either by increasing the inclination angle or by reducing the ambient pressure. Variations of the threshold angle required for the splash suppression as a function of the impact velocity were determined, as well as the threshold pressure as a function of the inclination angle and the impact velocity. The threshold pressure increases monotonically as the inclination angle increases for small enough impact velocities but varies in a nonmonotonic manner for high enough impact velocities. Modifications of the existing splash model permit the theoretical determination of the splash threshold conditions that agree well with the experimental observations. It is shown that it is the velocity of the lamella tip that determines the splash onset.

DOI: 10.1103/PhysRevLett.122.054501

Droplet splashes on dry smooth surfaces frequently occur in nature and can be found in a variety of industrial and agricultural applications. Examples include aerosol formation, combustion, spray coating, ink printing, and pesticide delivery [1–4]. Despite more than 140 years of study [5], there is a disagreement about the underlying mechanisms [1]. Theories based on the inertial dynamics [6–11], the Kelvin-Helmholtz instability [12–15], the air film dynamics [16–19], and the lamella aerodynamics [20–23] have been proposed. The inertial dynamics are unable to account for the effects of ambient pressure [21,24]. Recent studies [18,25–31] do not provide confirmation about the potential formation of an air film underneath the lamella tip before the splash initiation. A model based on the lamella aerodynamics [20] appears to be suitable for applications to a variety of conditions [20–22,32–35] and will be used in the present study. The majority of the existing studies are focused on the orthogonal impact while most impacts occurring in nature and in applications are oblique to the surface [1]. The oblique impact (see Fig. 1) started attracting attention more recently [13,36–38], nevertheless, its mechanism is still poorly understood and requires further investigations [1].

The suppression of the upward splash due to the increase of the inclination angle beyond a certain threshold $\alpha_{t,u}$ has already been reported in the literature [13,36–38]. The existence of another threshold angle $\alpha_{t,d}$, which results in a suppression of the downward splash for $\alpha > \alpha_{t,d}$, will be demonstrated during this investigation. It is well known that the droplet splash on a horizontal surface can be suppressed by reducing the ambient pressure below a certain threshold [24,39–43] as well as by using a moving surface [21]. Not surprisingly, the splash on an inclined surface can be suppressed in a similar manner. The required threshold pressure was measured for different combinations of the inclination angle α and the impact velocity V_0. It was found that the threshold pressure increases monotonically with increasing α but only for the low V_0's. When V_0 is large enough, the threshold pressure initially decreases and then begins to rapidly increase as α increases. The mechanisms responsible for these effects are described using a modified theoretical model validated through comparisons with the experimental data. It is shown that the onset of the droplet splash can be correlated with the velocity of the lamella tip at all pressures used in the experiment.

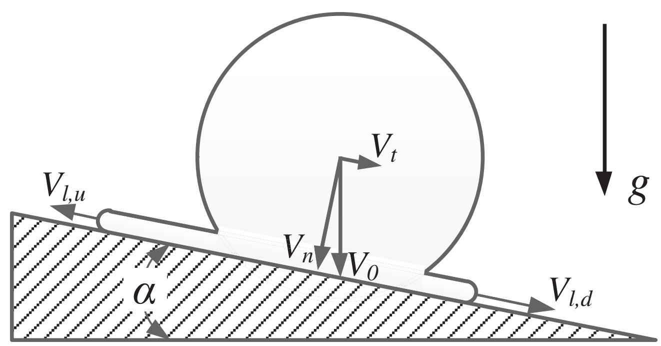

FIG. 1. Sketch of the droplet evolution during impact; α denotes the inclination angle, V_0 is the impact velocity, g is gravity, V_n and V_t stand for the normal- and tangential-to-the-surface impact velocity components, and $V_{l,u}$ and $V_{l,d}$ are the velocities of the upward and downward lamella tips, respectively.

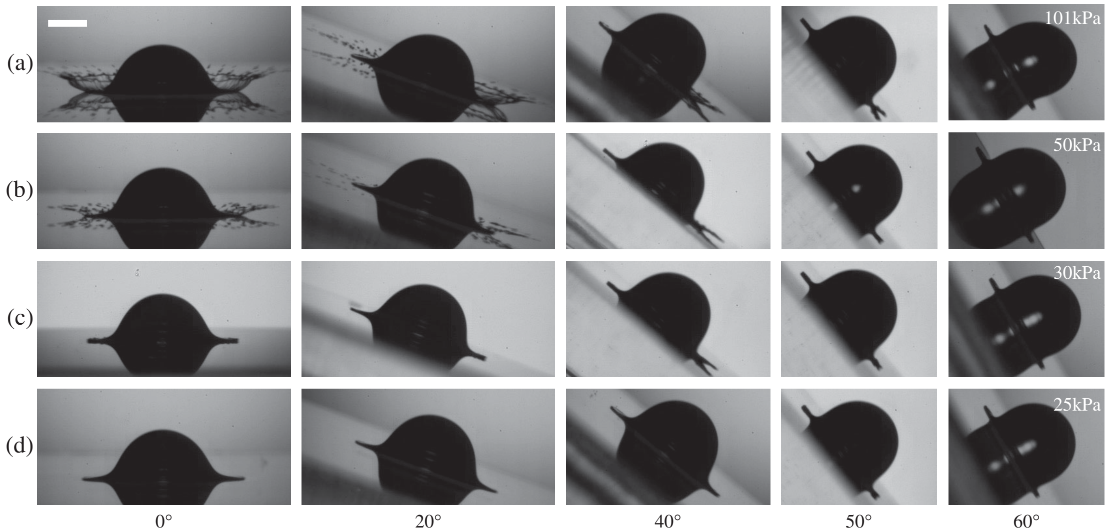

FIG. 2. Impacts of droplets released from the height $H = 0.46$ m. Rows and columns correspond to different pressures and angles, respectively. The images were taken at time $T = 0.4$ ms after the impact. (a) $P = 101$ kPa, $V_0 = 2.70$ m/s (We = 579): $\alpha = 0°$–$20°$ (double-side splash); $\alpha = 40°$–$50°$ (downward splash); $\alpha = 60°$ (spreading). (b) $P = 50$ kPa, $V_0 = 2.76$ m/s (We = 605): $\alpha = 0°$–$20°$ (double-side splash); $\alpha = 40°$ (downward splash); $\alpha = 50°$–$60°$ (spreading). (c) $P = 30$ kPa, $V_0 = 2.79$ m/s (We = 618): $\alpha = 0°$–$20°$ (spreading); $\alpha = 40°$ (downward splash); $\alpha = 50°$–$60°$ (spreading). (d) $P = 25$ kPa, $V_0 = 2.80$ m/s (We = 623); $\alpha = 0°$–$60°$ (spreading). The scale bar corresponds to 1.0 mm.

The experiments were conducted using ethanol of density $\rho = 791$ kg/m^3, dynamic viscosity $\mu = 1.19$ mPa s, and surface tension $\sigma = 22.9$ mN m^{-1} [21,24] with the ambient temperature of 24 ± 1 °C. Droplets with diameter $D_0 = 2.3 \pm 0.1$ mm were produced using a syringe pump and released from a height H above the surface. Variations of H provided the means for varying the impact velocity V_0 from 1.5 to 3.5 m/s, with the corresponding Weber number We $= \rho D_0 V_0^2/\sigma$ being in the range 179–973; this velocity was measured during experiments as it varies with the ambient pressure for the same H. On impact, the droplets were nearly spherical, with the aspect ratios (maximum height to width) being in the range of 0.95–1.05. Acrylic plates with the mean roughness amplitude of $R_a = 0.011$ μm [44] were used as the impact surfaces. The plates were placed on a rotary table whose inclination angle α was varied in the range 0°–90° with a precision of $\pm 0.1°$ (see Fig. 1). The experimental apparatus was placed in a transparent vacuum chamber whose pressure P could be varied in a range of 10–101 kPa. The impact was recorded using a Photron SA1.1 high-speed camera at rates of up to 100 000 fps and with a spatial revolution of up to 19.5 μm/pixel.

Figure 2 illustrates the effect of the inclination angle and the ambient gas pressure on the droplet splash. Each row represents a different pressure, and each column represents a different inclination angle. Both the upward and downward sides of the splash are inhibited by an increase of α for the ambient pressure $P = 101$ kPa. This is different from the splash on a moving surface [9,21], where the downstream splash is suppressed while the upstream splash is enhanced. An increase of α beyond the threshold $\alpha_{t,u}$ results in a complete suppression of the upward splash, as shown in the third panel in Fig. 2(a), which is consistent with the previous observations [13,36–38]. A further increase of α beyond another threshold angle $\alpha_{t,d}$ leads to a complete suppression of the downward splash, as shown in the last panel in Fig. 2(a).

The splash on a horizontal surface can be suppressed by reducing the ambient pressure below a certain threshold P_t, as shown in the first column of Fig. 2. The splash on an inclined surface can also be suppressed by reducing the ambient pressure, as demonstrated by images displayed in the three middle columns in Fig. 2. Interestingly, P_t decreases as α increases from 0° to 40° (see the first three columns in Fig. 2), whereas it increases rapidly as α increases from 40° to 60° (see the last three columns in Fig. 2).

We shall begin a detailed discussion of the effects of the inclination angle by focusing on the results for $P = 101$ kPa. Figure 3 illustrates variations of $\alpha_{t,u}$ and $\alpha_{t,d}$ as functions of the Weber number. Experiments for each data point were repeated at least three times. The double-sided splash occurs for $\alpha < \alpha_{t,u}$, the droplet spreading occurs for $\alpha > \alpha_{t,d}$, and the downward-only splash occurs for $\alpha_{t,u} < \alpha < \alpha_{t,d}$. The last situation is well illustrated in the third and the fourth column in Fig. 2(a). Both $\alpha_{t,u}$ and $\alpha_{t,d}$ increase monotonically with an increase in the Weber number.

To explain the effects of the inclination angle, we decompose the impact velocity V_0 into the normal-to-the-surface (V_n) and parallel-to-the-surface (V_t) components, i.e.,

$$V_n = V_0 \cos\alpha, \qquad V_t = V_0 \sin\alpha. \tag{1}$$

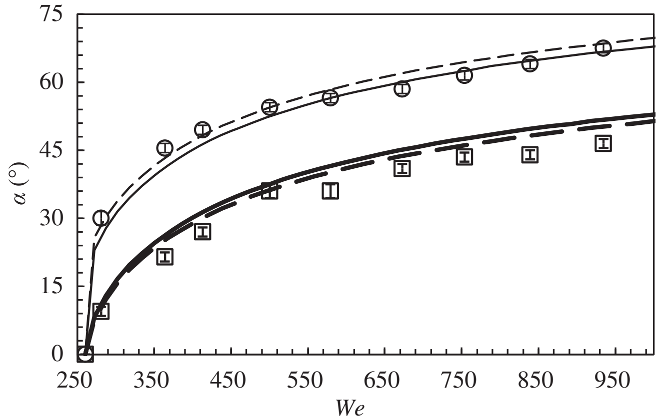

FIG. 3. Variations of the threshold angles $\alpha_{t,u}$ (squares and thick lines) and $\alpha_{t,d}$ (circles and thin lines) as functions of the Weber number We for the ambient pressure $P = 101$ kPa. Dashed and solid lines identify the theoretical results based either on the modified RG or on the simplified models, respectively. Symbols identify the experimental points. Error bars indicate the uncertainty.

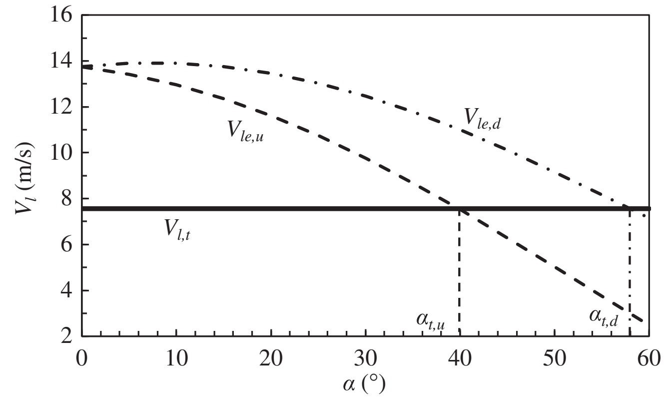

FIG. 4. Variations of the upward $V_{le,u}$ (dashed line) and the downward $V_{le,d}$ (dash-dotted line) lamella tip velocities determined from the modified RG model for We = 579 as functions of the inclination angle α. The solid line represents the threshold velocity $V_{l,t}$, and the thin dashed and dash-dotted lines identify $\alpha_{t,u}$ and $\alpha_{t,d}$, respectively.

As the droplet tends to flow down along the surface, the upward $(V_{l,u})$ and downward $(V_{l,d})$ lamella velocities can be approximately written as

$$V_{l,u} = V_l - V_t, \qquad V_{l,d} = V_l + V_t, \tag{2}$$

where V_l stands for the velocity of the lamella tip induced by V_n. V_l can be determined using the relation proposed by Riboux and Gordillo [20] (hereafter RG) of the form

$$V_l = \sqrt{3}/2\sqrt{D_0 V_n/2T}, \tag{3}$$

where T stands for time since the beginning of the impact. Similar relations with somewhat different coefficients were also proposed by Bird *et al.* [9] and Mandre *et al.* [16]. The substitution of (1) and (3) into (2) leads to

$$V_{l,u} = \sqrt{3}/2\sqrt{D_0 V_0 \cos\alpha/2T} - V_0 \sin\alpha,$$
$$V_{l,d} = \sqrt{3}/2\sqrt{D_0 V_0 \cos\alpha/2T} + V_0 \sin\alpha, \tag{4}$$

which can be used only for $T > T_e$, where T_e stands for the moment of initiation of the lamella formation. Splash is driven by the aerodynamic lift force proportional to the lamella tip velocity at T_e [9,16,20,45], i.e.,$V_{le,u}$ and $V_{le,d}$. The proper determination of T_e represents the central feature of the RG model [20]. The dimensionless lamella ejection time $t_e = 2T_e V_n/D_0$ can be calculated from the momentum balance [20] leading to a relation of the form

$$\sqrt{3}/2\,\mathrm{Re}^{-1} t_e^{-1/2} + \mathrm{Re}^{-2}\,\mathrm{Oh}^{-2} = 1.21 t_e^{3/2}, \tag{5}$$

where $\mathrm{Re} = \rho V_n D_0/2\mu$ is the Reynolds number and $\mathrm{Oh} = \mu/\sqrt{\rho D_0 \sigma/2}$ is the Ohnesorge number. Once t_e is determined, (3) gives V_{le} induced by V_n, and (4) gives both $V_{le,u}$ and $V_{le,d}$. Variations of $V_{le,u}$ and $V_{le,d}$ as functions of α for We = 579 displayed in Fig. 4 demonstrate that $V_{le,u}$ decreases with an increase of α, and this explains the suppression of the upward splash. The prediction of the downward splash is more complex as $V_{le,d}$ increases for $\alpha < 10°$ and then decreases.

The splash occurs only if the velocity of the lamella tip exceeds a certain threshold $V_{l,t}$. We take threshold information from the orthogonal impact, which is well known, and suppose that it determines the oblique impact as long as we replace V_0 with V_n. Variations of $V_{le,u}$ with α have already been determined analytically (see Fig. 4). If one begins with V_0 large enough to produce splashing at $\alpha = 0$, an increase of α decreases the effective impact velocity until $V_{le,u} = V_{l,t}$, which marks the beginning of the splash suppression. This point corresponds in Fig. 4 to the intersection of the line $V_{le,u}(\alpha)$ with the threshold $V_{l,t}$ and its location defines the threshold $\alpha_{t,u}$. The upward splashing is suppressed for $\alpha > \alpha_{t,u}$. Similar arguments lead to the determination of $\alpha_{t,d}$. The actual determination of the threshold conditions starts with the substitution of the known $V_{le,u}(= V_{l,t})$ into Eqs. (4) and (5) and determination of the corresponding $\alpha(= \alpha_{t,u})$. Results determined in this manner displayed in Fig. 3 (see dashed lines) agree well with the direct experimental measurements which suggests that the splash onset is indeed determined by the velocity of the lamella tip, as assumed in the theoretical model.

Typical values of the Ohnesorge number in the experiment were around 0.008, which justifies the use of the small-Oh approximation of (5) and results in an explicit relation for the lamella ejection time of the form

$$t_e \approx (1.1\mathrm{Re\,Oh})^{-4/3}. \tag{6}$$

The threshold angles determined using (6) are illustrated in Fig. 3 using solid lines. The agreement of the experimental

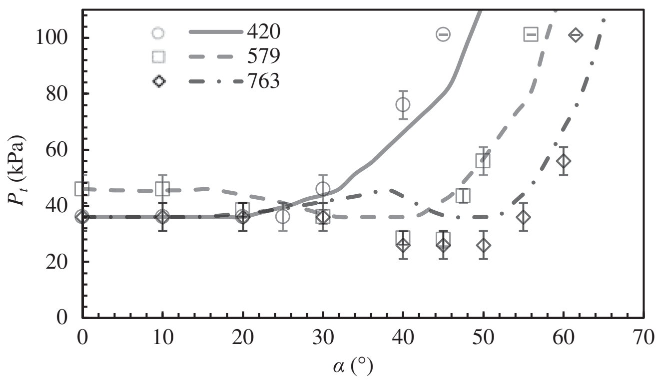

FIG. 5. Variations of the threshold pressure P_t as a function of the inclination angle α. The solid, dashed, and dash-dotted lines identify the theoretical predictions for We = 420, 579, 763, respectively, while symbols identify experimental points. Error bars indicate the uncertainty. Points on each curve furthest to the right were determined by measuring $\alpha_{t,d}$ for the fixed pressure $P_t = 101$ kPa and therefore have no error bars.

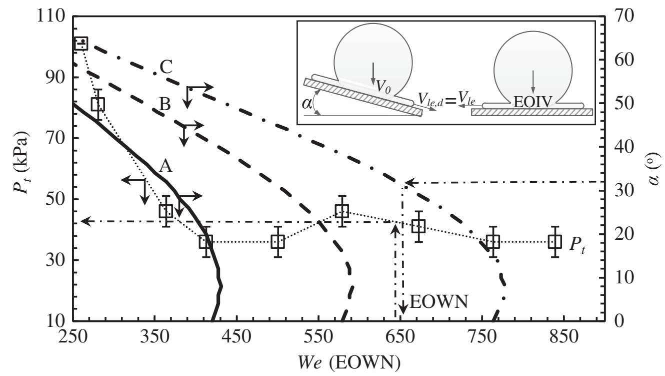

FIG. 6. Squares identify experimentally determined variations of the threshold pressure P_t as a function of the Weber numbers We for the orthogonal impact. Error bars indicate the experimental uncertainty. The thick lines illustrate variations of the equivalent orthogonal Weber number (EOWN) computed from the equivalent orthogonal impact velocity (EOIV) as a function of the inclination angle α; lines A, B, C correspond to the oblique impacts with We = 420, 579, 763, respectively. The arrows on the thin dash-dotted line illustrate information flow used in the determination of the threshold pressure for the oblique impact using information about the orthogonal impact and the available theory (see text for details). The solid arrows point to the relevant axes. The inset provides definitions of quantities used in the process of determination of EOIV.

data with the modified RG model justifies the use of the simplified method.

We shall now turn our attention to the effects of ambient pressure. Our observations show that splash on an inclined surface can also be completely suppressed by reducing the ambient pressure. The required threshold P_t was measured for three We's as a function of α and the results are displayed in Fig. 5. We used the downward splash to determine P_t as it is stronger and thus easier to observe. The measurements were repeated at least three times for each data point and the thresholds required for the complete splash suppression were determined with the uncertainty not bigger than ± 5 kPa. In the case of the two larger Weber numbers (We = 579, 763), P_t initially decreases with α until $\alpha \approx 45°$ and then it rapidly increases, while for the smallest Weber number (We = 420) it monotonically increases over the whole range of α considered in this study. One may further note that the thresholds for the orthogonal impacts ($\alpha = 0°$) are the same for We = 420 and We = 763 but lower than the threshold for the middle Weber number We = 579. These thresholds increase monotonically as We is reduced for impacts with large inclination angles ($\alpha > 45°$).

To explain variations of the threshold pressure, the threshold pressure for the orthogonal impact was measured experimentally for V_0 in the range 1.8 to 3.3 m/s, with corresponding We in the range 257 to 865, as shown in Fig. 6. P_t varies nonmonotonically with We as previously observed [24]. It rapidly decreases when We increases to 420, then slowly increases as We increases to about 579 and then it decreases again. The processes responsible for the formation of the maximum are not understood [24] and their explanation is beyond the scope of this Letter.

We assume that the threshold lamella velocities, which mark the transition between the splash and no splash situations, are the same for the orthogonal and oblique impacts at the same pressure. One needs to use this assumption to determine the equivalent orthogonal impact velocity (EOIV) which gives the same lamella velocity at the transition point and use this information to predict the oblique P_t from the known orthogonal P_t. In the analysis we used the downward lamella as the oblique P_t was determined by it. As shown in the inset in Fig. 6, the process starts with selection of a particular oblique impact, i.e., (α, V_0), and relies on the use of (3)–(5) to determine $V_{le,d}$. Since the same lamella velocity must be produced by the orthogonal impact, we determine EOIV from (3)–(5) using known $V_{le} (= V_{le,d})$. Subsequently, the equivalent orthogonal Weber number (EOWN) is computed by replacing the V_0 with EOIV which leads to three thick lines displayed in Fig. 6, one for each of the three Weber numbers used in the experiment (We = 420, 579, 763). The process ends with the determination of P_t for the oblique impact from the experimental data for $\alpha = 0°$ displayed in Fig. 6 at We(= EOWN). The direction of the information flow is illustrated in Fig. 6 for the largest Weber number used in the experiments. Results displayed in Fig. 5 demonstrate good agreement between P_t's determined directly in the experiment with those predicted theoretically using information about orthogonal P_t's. The above arguments and good agreement with the experiment suggest that the lamella tip velocity does indeed determine the splash onset for all pressures.

The nonmonotonic variations of P_t for the two higher Weber numbers occurring over different ranges of α and monotonic variations for the smallest Weber number used in the experiments shown in Fig. 5 require some discussion. Since the lift force is proportional to pressure when all other conditions remain the same [20,45], one would expect P_t to exhibit variations qualitatively similar to those of EOWN's which increase slightly when α increases up to about 10° and then decrease rapidly (see Fig. 6). The local minimum of P_t for the largest Weber number (We = 763) occurs for $\alpha \approx 55°$ (see Fig. 5), which corresponds to the zone of EOWN where P_t for the orthogonal impact has a local minimum (see Fig. 6). The local minimum of P_t for the middle Weber number (We = 579) occurs for $\alpha \approx 35°$, which corresponds to the same zone of EOWN, i.e., the zone where P_t for the orthogonal impact has a local minimum. There is no local minimum of P_t for the smallest Weber number (We = 420; see Fig. 5) and variations of the corresponding EOWN overlap with the zone where the orthogonal P_t varies monotonically. It can be concluded that the mechanics of the nonmonotonic variations of P_t observed in the oblique impact are very similar to those of the orthogonal impact.

To conclude, we experimentally observed that the droplet splashing can be entirely suppressed by either increasing the inclination angle or reducing the ambient pressure. The threshold angle increases monotonically with an increase in the Weber number. The nonmonotonic variations of the threshold pressure as a function of the inclination angle are observed for higher Weber numbers. The mechanisms responsible for these phenomena are described using a theoretical model validated through comparisons with the experimental data. Results demonstrate that it is the velocity of the lamella tip that determines the splash onset. We note that the arguments based only on the aerodynamics are unable to explain the nonmonotonic variations of the threshold pressure as a function of the inclination angle for higher Weber numbers. It is possible that other factors, like the Kelvin-Helmholtz instability and the air film dynamics, play a role during the splash process. However, our current experimental setup cannot give information on the dynamics of the air film underneath the lamella. This question deserves more attention in the future.

The authors would like to thank Professor S. Ma and Dr. Q. Ma for kindly providing us the high-speed camera. J. H. especially thanks Professor S. I. Green for introducing him to the subject. This study was financially supported by the National Natural Science Foundation of China under Grant No. 51406012 and 111 Project under Grant No. B16003.

*hjgizq@bit.edu.cn

[1] C. Josserand and S. T. Thoroddsen, Annu. Rev. Fluid Mech. **48**, 365 (2016).
[2] A. L. Yarin, Annu. Rev. Fluid Mech. **38**, 159 (2006).
[3] S. T. Thoroddsen, T. G. Etoh, and K. Takehara, Annu. Rev. Fluid Mech. **40**, 257 (2008).
[4] G. Liang and I. Mudawar, Int. J. Heat Mass Transfer **106**, 103 (2017).
[5] A. M. Worthington, Proc. R. Soc. London **25**, 261 (1876).
[6] C. D. Stow and M. G. Hadfield, Proc. R. Soc. A **373**, 419 (1981).
[7] C. Mundo, M. Sommerfeld, and C. Tropea, Int. J. Multiphase Flow **21**, 151 (1995).
[8] R. E. Pepper, L. Courbin, and H. A. Stone, Phys. Fluids **20**, 082103 (2008).
[9] J. C. Bird, S. Tsai, and H. A. Stone, New J. Phys. **11**, 063017 (2009).
[10] S. T. Thoroddsen, K. Takehara, and T. G. Etoh, J. Fluid Mech. **706**, 560 (2012).
[11] C. J. Howland, A. Antkowiak, J. R. Castrejón-Pita, S. D. Howison, J. M. Oliver, R. W. Style, and A. A. Castrejón-Pita, Phys. Rev. Lett. **117**, 184502 (2016).
[12] L. Xu, Phys. Rev. E **75**, 056316 (2007).
[13] J. Liu, H. Vu, S. S. Yoon, R. Jepsen, and G. Aguilar, Atomization Sprays **20**, 297 (2010).
[14] Y. Liu, P. Tan, and L. Xu, Proc. Natl. Acad. Sci. U.S.A. **112**, 3280 (2015).
[15] Z. Jian, C. Josserand, S. Popinet, P. Ray, and S. Zaleski, J. Fluid Mech. **835**, 1065 (2018).
[16] S. Mandre, M. Mani, and M. P. Brenner, Phys. Rev. Lett. **102**, 134502 (2009).
[17] S. Mandre and M. P. Brenner, J. Fluid Mech. **690**, 148 (2012).
[18] J. M. Kolinski, S. M. Rubinstein, S. Mandre, M. P. Brenner, D. A. Weitz, and L. Mahadevan, Phys. Rev. Lett. **108**, 074503 (2012).
[19] L. Duchemin and C. Josserand, C.R. Mec. **340**, 797 (2012).
[20] G. Riboux and J. M. Gordillo, Phys. Rev. Lett. **113**, 024507 (2014).
[21] J. Hao and S. I. Green, Phys. Fluids **29**, 012103 (2017).
[22] G. Riboux and J. M. Gordillo, Phys. Rev. E **96**, 013105 (2017).
[23] A. M. P. Boelens and J. J. de Pablo, Phys. Fluids **30**, 072106 (2018).
[24] L. Xu, W. W. Zhang, and S. R. Nagel, Phys. Rev. Lett. **94**, 184505 (2005).
[25] M. M. Driscoll and S. R. Nagel, Phys. Rev. Lett. **107**, 154502 (2011).
[26] R. C. A. van der Veen, T. Tran, D. Lohse, and C. Sun, Phys. Rev. E **85**, 026315 (2012).
[27] Y. Liu, P. Tan, and L. Xu, J. Fluid Mech. **716**, R9 (2013).
[28] J. de Ruiter, D. van den Ende, and F. Mugele, Phys. Fluids **27**, 012105 (2015).
[29] E. Q. Li and S. T. Thoroddsen, J. Fluid Mech. **780**, 636 (2015).
[30] H. Y. Lo, Y. Liu, and L. Xu, Phys. Rev. X **7**, 021036 (2017).
[31] E. Q. Li, K. R. Langley, Y. S. Tian, P. D. Hicks, and S. T. Thoroddsen, Phys. Rev. Lett. **119**, 214502 (2017).
[32] H. J. J. Staat, T. Tran, B. Geerdink, G. Riboux, C. Sun, J. M. Gordillo, and D. Lohse, J. Fluid Mech. **779**, R3 (2015).
[33] G. Riboux and J. M. Gordillo, J. Fluid Mech. **772**, 630 (2015).
[34] G. Riboux and J. M. Gordillo, J. Fluid Mech. **803**, 516 (2016).
[35] T. C. de Goede, N. Laan, K. G. de Bruin, and D. Bonn, Langmuir **34**, 5163 (2018).

[36] Š. Šikalo, C. Tropea, and E. N. Ganic, J. Colloid Interface Sci. **286**, 661 (2005).
[37] L. Courbin, J. C. Bird, and H. A. Stone, Chaos **16**, 041102 (2006).
[38] D. G. K. Aboud and A.-M. Kietzig, Langmuir **31**, 10100 (2015).
[39] L. Xu, L. Barcos, and S. R. Nagel, Phys. Rev. E **76**, 066311 (2007).
[40] P. Tsai, R. C. A. van der Veen, M. van de Raa, and D. Lohse, Langmuir **26**, 16090 (2010).
[41] A. Latka, A. Strandburg-Peshkin, M. M. Driscoll, C. S. Stevens, and S. R. Nagel, Phys. Rev. Lett. **109**, 054501 (2012).
[42] C. S. Stevens, Eur. Phys. Lett. **106**, 24001 (2014).
[43] C. S. Stevens, A. Latka, and S. R. Nagel, Phys. Rev. E **89**, 063006 (2014).
[44] J. Hao, Phys. Fluids **29**, 122105 (2017).
[45] J. B. T. Moulson and S. I. Green, Phys. Fluids **25**, 102106 (2013).